

Quantum signatures and semiclassical limitations in the transmission of Fock states

D. J. Nader¹

¹*Department of Optics, Faculty of Science, Palacký University, Olomouc 77146, Czech Republic*

Transmission through potential barriers is a fundamental problem in quantum mechanics. While semiclassical methods can approximate certain aspects of transmission, they fail to capture the intrinsically quantum interference associated with Wigner-function negativity. We numerically study the transmission of displaced Fock states through an inverted-oscillator barrier, with and without a Kerr nonlinearity that offers a potential route to experimental realization. These states allow only an approximate classical description, since their characteristic Wigner-function negativity is absent in phase space. The semiclassical simulation reproduces the overall transmission but deviate from exact results and fail to capture short-time plateaus that arise when regions of Wigner-function negativity cross the barrier. With the Kerr nonlinearity, reflections from nonlinear boundaries drive interference into classically forbidden regions, an effect that is inaccessible to semiclassical approaches. We find that these interference effects do not alter the maximum transmission probability, which is bounded by the initial positive-energy fraction and therefore already encoded in the phase-space structure of the Fock states. Because Fock states cannot be faithfully represented within classical phase space, the transmission through a barrier reveals fundamental limitations of semiclassical approaches.

I. INTRODUCTION

One of the most intriguing phenomena in quantum mechanics is the transmission of particles through potential barriers higher than their kinetic energy, a process known as quantum tunneling [1]. Since the early days of quantum theory, tunneling has played a central role in explaining molecular spectra [2], electron emission from metals [3], and α -decay in nuclei [4]. Currently, tunneling phenomena can be simulated on different experimental platforms, such as NMR systems with a few spin nuclei [5], superconducting circuits [6, 7] and Bose-Einstein Condensates with ultracold atoms [8]. On the theoretical side, tunneling has been studied extensively, especially in double-well potentials [9–13], but also in continuous-variable systems [14, 15], spin models [16, 17], and Bose-Einstein condensates [18, 19].

Many features of tunneling—such as wavepacket transmission and energy-level splitting—can be accurately captured using semiclassical approximations [20–26]. However, semiclassical approaches cannot account for Wigner function negativity [27], a genuine quantum feature with no classical analogue. From a practical perspective, Wigner negativity has been proposed as a necessary ingredient for outperforming classical devices [28–30]. It is well established that the fine structure of the Wigner function—particularly its negativity and interference fringes—is closely connected to the sensitivity of quantum states to rotations and displacements [31]. Despite growing interest, the precise role of Wigner negativity in tunneling and transmission phenomena, and its broader implications for nonclassical physics, remains under discussion [32–35]. In this context, marginal distributions are especially relevant for studying quantum barrier transmission, including contributions that may be associated with tunneling, since they correspond to directly measurable observables accessible through modern quantum state reconstruction techniques [36–39].

In this work, we examine to what extent the transmission effect can be captured semiclassically using phase-space distributions. To this end, we compare two approaches: the ex-

act Wigner function and the Truncated Wigner Approximation (TWA) [40–43], a semiclassical method that, by construction, neglects negative values. Because Fock states exhibit pronounced Wigner-function negativity [44], they provide natural test cases—unlike Gaussian states [45] with strictly positive Wigner functions—for examining the differences between classical and quantum phase-space descriptions and their consequences for the transmission phenomenon. Our analysis starts with displaced Fock states evolving in an inverted oscillator, where the initial Wigner negativity remains constant due to the absence of nonlinear interactions. We then extend the study to the inverted oscillator with Kerr nonlinearity [46], a system of significant experimental relevance [47, 48], which offers a viable route for testing the findings on currently available platforms.

sectionModels and Hamiltonians

In this section, we introduce two models for studying the transmission of displaced Fock states. The first is the inverted harmonic oscillator, which admits an analytical treatment, while the second extends it by including a small Kerr nonlinearity. The former serves as a fundamental model, whereas the latter is experimentally more accessible and incorporates nonlinear interactions.

A. Inverted Harmonic Oscillator

The inverted oscillator (IO) [49] provides the simplest example of a potential barrier [49–51]. Its Hamiltonian is given by

$$\hat{H} = \frac{1}{2}(\hat{p}^2 - \hat{q}^2) = -\frac{1}{2}(\hat{a}^{\dagger 2} + \hat{a}^2), \quad (1)$$

where \hat{q} and \hat{p} are the canonical position and momentum operators, and \hat{a}, \hat{a}^\dagger are the usual bosonic annihilation and creation operators.

In classical mechanics, the inverted oscillator potential has a maximum at energy $E = 0$. Particles with $E < 0$ are reflected, while those with $E > 0$ pass over the barrier [51]. In

quantum mechanics, the inverted oscillator generates squeezing [52] and has been used to investigate exponential delocalization [53, 54] as well as quantum–classical correspondence [55]. Analyzing the dynamics of quantum states in the inverted oscillator is particularly challenging because the associated phase space is unbounded [55].

In this work, the dynamics is initialized with displaced Fock states $\hat{D}(\alpha)|n\rangle$, where the displacement operator is defined as $\hat{D}(\alpha) = \exp(\alpha\hat{a}^\dagger - \alpha^*\hat{a})$ and the displacement parameter as $\alpha = \frac{1}{\sqrt{2}}(\bar{q} + i\bar{p})$. A key property for our analysis is that the mean energy

$$\begin{aligned} \bar{E} &= \langle n|\hat{D}^\dagger(\alpha)\hat{H}\hat{D}(\alpha)|n\rangle \\ &= -(|\text{Re}(\alpha)|^2 - |\text{Im}(\alpha)|^2), \end{aligned} \quad (2)$$

is independent of the Fock index n and only depends on the displacement parameter α . This follows directly from the operator identities [56] $\hat{D}^\dagger(\alpha)\hat{a}\hat{D}(\alpha) = \hat{a} + \alpha$ and $\hat{D}^\dagger(\alpha)\hat{a}^\dagger\hat{D}(\alpha) = \hat{a}^\dagger + \alpha^*$. Consequently, the mean energy (2) can be tuned below the barrier top ($E_c = 0$) by choosing the displacement parameter such that $|\text{Im}(\alpha)| < |\text{Re}(\alpha)|$.

B. Inverted oscillator with a Kerr nonlinearity

To address experimentally relevant scenarios, we extend our analysis to the inverted oscillator with a Kerr nonlinearity [46, 57, 58]. The Hamiltonian is the following

$$\hat{H} = -\varepsilon_2(\hat{a}^{\dagger 2} + \hat{a}^2) + K\hat{a}^{\dagger 2}\hat{a}^2, \quad (3)$$

where ε_2 denotes a parametric driving strength and K denotes the Kerr nonlinearity. This model is experimentally available with mechanical oscillators [47], superconducting circuits [48, 59, 60] and atoms in microcavities. [61]. On the theoretical side, it has been employed to study quantum tunneling [14, 46], quantum phase transitions [62], quantum-state engineering [57, 63], and a broad range of other quantum phenomena [58, 64–68].

In the semiclassical limit, we express the Hamiltonian in terms of canonical variables (q, p)

$$H = \varepsilon_2(p^2 - q^2) + \frac{K}{4}(q^2 + p^2)^2. \quad (4)$$

For $K = 0$ and $\varepsilon_2 = 1/2$, the Hamiltonian (4) reduces to the inverted oscillator (1). For $K > 0$, the nonlinearity generates effective outer walls, and the resulting phase-space structure resembles that of a double-well potential with a separatrix at the critical energy ($E_c = 0$).

Figure 1 shows the classical trajectories in phase space, including the separatrix (green) at the critical energy $E_c = 0$ [69, 70], sub-barrier trajectories (blue), and super-barrier trajectories (red). Near the origin, the trajectories closely resemble those of the inverted oscillator [51], providing a convenient baseline for comparison.

In the presence of the Kerr nonlinearity, the mean energy of displaced Fock states

$$\bar{E} = -(|\text{Re}(\alpha)|^2 - |\text{Im}(\alpha)|^2) + K(|\alpha|^4 + n(n-1) + 4n|\alpha|^2), \quad (5)$$

depends explicitly on the Fock index n . To maintain the initial states at the same energy below the threshold $E_c = 0$, the displacement parameter α must therefore be adjusted as a function of n .

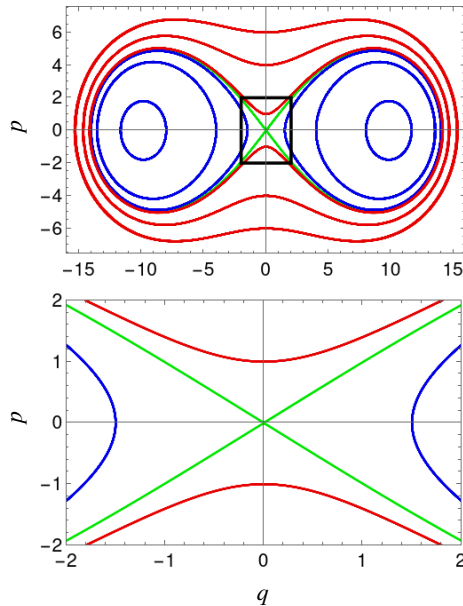


Figure 1. Classical trajectories of the inverted oscillator with a small Kerr nonlinearity (4). The configuration of parameters is $\varepsilon_2 = 1/2$ and $K = 10^{-2}$. The green trajectory is the separatrix at the critical energy ($E_c = 0$) corresponding to the top of the inverted oscillator. The blue/red trajectories correspond to energies smaller/larger than the top of the inverted oscillator ($E_c = 0$). The bottom panel is a zoom into the center of the phase space in the top panel delimited by the square. At this small portion of the phase space the trajectories resemble those of the inverted oscillator [51].

II. QUANTUM DYNAMICS IN THE PHASE SPACE

We focus on the dynamics of displaced Fock states, $|\psi_0\rangle = D(\alpha)|n\rangle$ in the inverted oscillator with and without Kerr nonlinearity. The preparation of such states is currently feasible with atoms in cavities [71] and in superconducting circuits [72]. For simplicity, we consider initial states localized on the left side of the inverted oscillator, with displacement parameter $\text{Re}(\alpha) < 0$ and mean energy smaller than the top of the inverted oscillator $\bar{E} < 0$.

To investigate the dynamics in phase space, we employ two complementary methods: A) the exact Wigner function and B) the Truncated Wigner Approximation (TWA). Both approaches are described in detail below.

A. Quantum approach: Wigner function

The Wigner function is a quasi-probability distribution that provides a phase-space representation of quantum states. It is

defined as [27, 73]

$$W(q, p, t) = \frac{1}{\pi} \int \langle q+y | \psi(t) \rangle \langle \psi(t) | q-y \rangle e^{2ipy} dy, \quad (6)$$

where $|\psi(t)\rangle$ is the wave function. By integrating over momentum, the Wigner function yields the correct marginal probability distribution [74]:

$$P(q, t) = \int W(q, p, t) dp = |\Psi(q, t)|^2. \quad (7)$$

Since the Wigner function (6) can take negative values, it is not a true probability distribution in the classical sense [73]. However, this negativity is not a flaw, but rather a fundamental feature that reflects quantum interference in phase space [75]. It is often interpreted as a signature of nonclassicality or quantum coherence [44] and it is typically quantified as $\delta(t) = \int (|W(q, pt, t)| - W(q, p, t)) dx dp$.

For closed systems with initial pure states, the unitary evolution of the wave function is given by

$$\psi(t) = \hat{U}(t) |\psi_0\rangle, \quad \hat{U} = \exp\left(-\frac{i}{\hbar} \hat{H} t\right).$$

Some particular cases of interest are the class of coherent states $|\alpha\rangle = D(\alpha)|0\rangle$ whose Wigner functions are Gaussian [76] and everywhere positive, allowing them to be interpreted as classical-like probability distributions. The transmission probability for a particle to be found in the region Ω can be obtained through marginal probability (7) as

$$P(\Omega, t) = \int_{-\infty}^{\infty} \int_{q_1}^{q_2} W(q, p, t) dq dp, \quad (8)$$

where q_1 and q_2 are the boundaries of the region Ω . For concreteness, we focus on states initially displaced to the left of the inverted oscillator and evaluate the probability of finding the particle on the right side, corresponding to $q_1 = 0$ and $q_2 = \infty$.

In the case of the pure inverted oscillator (1)—in the absence of nonlinear forces—the negativity of the initial state remains constant under time evolution [77] $\delta(t) = \delta(t=0)$. This makes the inverted oscillator an ideal model to explore how the initial state's nonclassical features influence the transmission probabilities. However, the quantum states in this system undergo exponential delocalization over time [53], in addition to the unbound phase space that prevents the numerical convergence of the integral (8) at large times. In contrast, the Kerr nonlinearity (3) represents a nonlinear force that effectively bounds the phase space by creating effective outer walls. This confinement enables stable numerical evaluation of the transmission probabilities (8) at longer times. Nevertheless, the nonlinear terms in the Kerr Hamiltonian (3) modify the negativity of the initial state $\delta(t) \neq \delta(t=0)$, leading to the emergence of interference patterns during the evolution, even for initially Gaussian states, whose Wigner functions are positive everywhere at $t=0$.

To quantify how much of each initial state lies above the top of the inverted harmonic potential, we introduce a semiclassical measure of the population in the region of positive

classical energy,

$$P_0(E > 0) = \iint \Theta(H(q, p) - E_c) W(q, p, t=0) dq dp, \quad (9)$$

where $E_c = 0$ and $\Theta(x)$ is the Heaviside step function,

$$\Theta(x) = \begin{cases} 0, & x < 0, \\ 1, & x \geq 0. \end{cases} \quad (10)$$

The quantity $P_0(E > 0)$ represents the positive-energy fraction of the initial Wigner distribution. However, (9) should not be interpreted as an exact quantum probability, because the classical step function $\Theta(H(q, p))$ does not coincide with the Weyl symbol of the corresponding quantum projector $\Theta(\hat{H})$ (see, e.g., [27, 73]). Nevertheless, it provides a convenient semiclassical reference for estimating the fraction of the initial Wigner distribution located in a different region of trajectories in the phase space (see Figure 1).

B. Semiclassical approach: TWA

Alternatively, the dynamics of quantum states can be simulated using the truncated Wigner approximation (TWA) [40, 41, 43]. This semiclassical method leverages the stochastic nature of quantum mechanics by generating an ensemble of N points in classical phase space that collectively approximate the Wigner function of the initial quantum state. Each point in this ensemble evolves independently according to Hamilton's equations of motion

$$\dot{q} = \frac{\partial H}{\partial p}, \quad \dot{p} = -\frac{\partial H}{\partial q}, \quad (11)$$

where H denotes the classical Hamiltonian. For initial coherent states $|\psi_0\rangle = \hat{D}(\alpha)|0\rangle$, the Wigner function is strictly positive and can be directly interpreted as a classical probability distribution. In contrast, for displaced Fock states $D(\alpha)|n\rangle$, which exhibit Wigner negativity, an additional approximation is required to generate a positive-definite sampling distribution. To address this, we employ a Gaussian approximation [78] for Fock states, defined as

$$P_n(q, p) = \sqrt{\frac{2}{\pi}} \exp\left(-\frac{(q^2/2 + p^2/2 - n - 1/2)^2}{1/2}\right), \quad (12)$$

where n is the Fock state index. This distribution approximates the Wigner function of the initial displaced Fock state and is used to generate the initial ensemble for TWA simulations, as illustrated in Figure 5.

Within the TWA framework, only those phase-space points (q_i, p_i) , with positive energy $E(q_i, p_i) > 0$ exceeding the top of the inverted oscillator, can contribute to the transmission probability into the region Ω delimited by the turning points $q_{1,2}$. The transmission probability is then estimated using the Heaviside step function

$$P(\Omega, t) = \frac{1}{N} \sum_{i=1}^N \Theta(q_i(t) - q_1) - \frac{1}{N} \sum_{i=1}^N \Theta(q_i(t) - q_2). \quad (13)$$

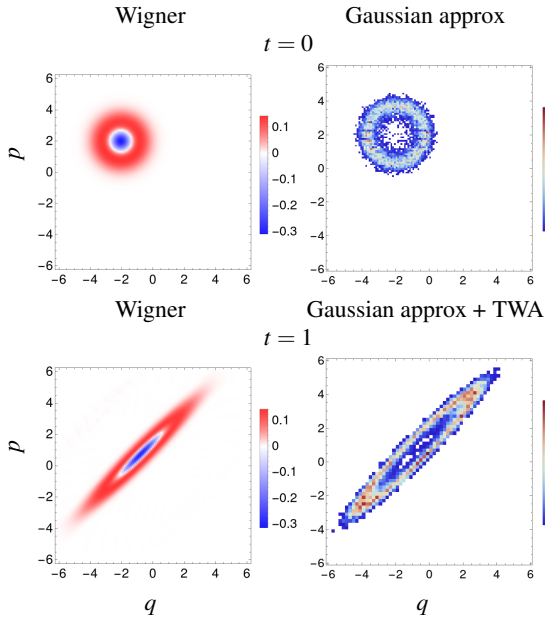


Figure 2. (Left column) Displaced Fock state $D(\alpha)|1\rangle$ with displacement parameter $\alpha = \frac{1}{2}(-2 + 2i)$ at different times evolving in the inverted oscillator (1). (Right column) Histogram of the set of $N = 10^5$ points that replicate the Fock state according to the Gaussian approximation (12).

This approach is particularly advantageous for avoiding the direct evaluation of the Wigner function integral in (8), especially in regimes where numerical convergence is challenging. However, by construction, the TWA does not account for negative regions of the Wigner function and therefore cannot capture quantum interference effects associated with Wigner negativity.

III. RESULTS

A. Coherent states in the inverted oscillator

For the specific case of a coherent state evolving under the inverted harmonic oscillator, the transmission probability given in (8) can be evaluated analytically. In the absence of nonlinear forces, the dynamics of the Wigner function is entirely classical, in the sense that it obeys the Liouville equation [73]

$$\frac{\partial W}{\partial t} = -p \frac{\partial W}{\partial q} + \frac{\partial U}{\partial q} \frac{\partial W}{\partial p}. \quad (14)$$

The solution at a later time t is obtained by following the classical trajectories backward in time $W(q, p, t) = W(q_{-t}(q, p), p_{-t}(q, p), 0)$ where q_t and p_t are the classical trajectories governed by Hamilton's equations of motion (11). For the inverted oscillator, these trajectories take the form

[79, 80]

$$\begin{aligned} q_t &= q \cosh(t) + p \sinh(t) \\ p_t &= p \cosh(t) + q \sinh(t). \end{aligned} \quad (15)$$

Using these expressions, the time-evolved Wigner function of an initial coherent state centered at (q_0, p_0) becomes

$$W(q, p, t) = \frac{1}{\pi} e^{-(q \cosh(-t) + p \sinh(-t) - q_0)^2} e^{-(p \cosh(-t) + q \sinh(-t) - p_0)^2}. \quad (16)$$

Substituting (16) into (8) yields an integral that can be solved analytically using the error function [81]. The resulting expression for the transmission probability is

$$P(q > 0, t) = \frac{1}{2} (1 - \operatorname{erf}(-c(t))), \quad (17)$$

$$\text{where } c(t) = \frac{q_0 \cosh(t) + p_0 \sinh(t)}{\sqrt{\cosh^2(t) + \sinh^2(t)}}.$$

Figure 3 shows the time evolution of the transmission probability $P(q > 0, t)$ for an initial coherent state with displacement parameter $\alpha = \frac{1}{\sqrt{2}}(-3 + 2.5i)$. The probability increases smoothly over time and asymptotically approaches roughly $P_0(E > 0) = 0.308$. The transmission probability from the TWA (13) is found to be in good agreement with the exact analytical result (17). At $t = 4$, the exact transmission probability $P_{\text{ex}}(x > 0, t = 4) = 0.308$ while the TWA gives a slightly lower value $P_{\text{TWA}}(x > 0, t = 4) = 0.299$. This correspondence is expected, since in the absence of nonlinear forces the state remains Gaussian throughout its evolution [73], and its dynamics can be accurately captured by classical phase space trajectories.

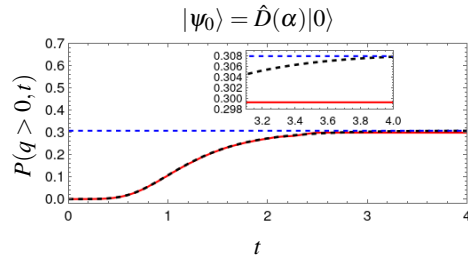


Figure 3. Probability $P(q > 0, t)$ of finding the particle in the right side of the inverted oscillator as a function of the time. The solid red line corresponds to the TWA and the black dashed line to the exact analytical formula (17). The blue dashed line represents the probability $P_0(E > 0) = 0.308$. The initial state is a coherent state $|\psi_0\rangle = \hat{D}|0\rangle$ with displacement parameter $\alpha = \frac{1}{\sqrt{2}}(-3 + 2.5i)$.

B. Displaced Fock states in the inverted oscillator

More interesting are the initial displaced Fock states $|\psi_0\rangle = |\hat{D}(\alpha)|n\rangle$, with Fock index $n \neq 0$, which exhibit significant Wigner function negativity. For these non-Gaussian states, the transmission probability (8) must be evaluated numerically, and can be computed with the target accuracy of 10^{-6} only

for short times $t < 1.6$, due to the increasing delocalization of the Wigner function.

Figure 4 shows the time evolution of the transmission probability $P(q > 0, t)$ for different initial displaced Fock states. According to (2), displaced Fock states with the same displacement parameter share the same mean energy. For the analysis we chose $\alpha = \frac{1}{\sqrt{2}}(-3 + 2.5i)$. The agreement between the exact numerical results and the TWA method is good at short times. However, the exact dynamics display short-time plateaus in the tunneling probability that are absent in the TWA. The instantaneous Wigner functions shown in the insets of Figure 4 reveal that these plateaus arise when the negative regions of the Wigner function cross into the right side of the inverted oscillator. The corresponding marginal distributions indicate that these features are associated with zeros of the probability distribution crossing the inverted oscillator. This effect cannot be captured within a classical phase-space description.

Although there are indications that the transmission probabilities obtained from the exact Wigner dynamics and from the TWA may converge to different asymptotic values, this cannot be confirmed within the present model because the rapid delocalization of the states prevents the convergence of the transmission integral (8). In all cases, however, the exact transmission probability $P(x > 0, t)$ does not exceed the initial positive-energy fraction $P_0(E > 0)$, contrary to the results from the TWA. When the Kerr nonlinearity is included, the phase space becomes effectively bounded, and the integrals defining the asymptotic probabilities are expected to converge, allowing for more reliable quantitative comparisons.

C. Displaced Fock states in the inverted oscillator with a small Kerr nonlinearity

The analysis of the time evolution of displaced states can be extended to the inverted oscillator with a small Kerr nonlinearity (3). In this case, the Kerr nonlinearity K introduces effective outer boundaries in phase space, together with nonlinear forces that can distort the negative regions of the Wigner function. For small values of K , the dynamics remain close to those of the inverted harmonic oscillator over short time scales. At longer times, however, the effective boundaries drive the state along the separatrix and eventually produce a bouncing effect.

As an example, Figure 5 shows the exact Wigner function and the corresponding Gaussian approximation + TWA simulation at selected times for the initial displaced Fock state $\hat{D}(\alpha)|1\rangle$. For short times ($t \lesssim 1$), the state is squeezed, just as it is in the pure inverted oscillator (see Figure 5). At longer times, however, the state follows the curvature of the separatrix of the inverted Kerr oscillator, reflecting the presence of effective boundaries imposed by the Kerr nonlinearity. The exact Wigner function penetrates into the right-hand side of the separatrix, Ω_r , giving rise to interference patterns. The interference in the right side of the separatrix corresponds to transmission through classically forbidden regions, while those in the left side may be associated with partial reflection

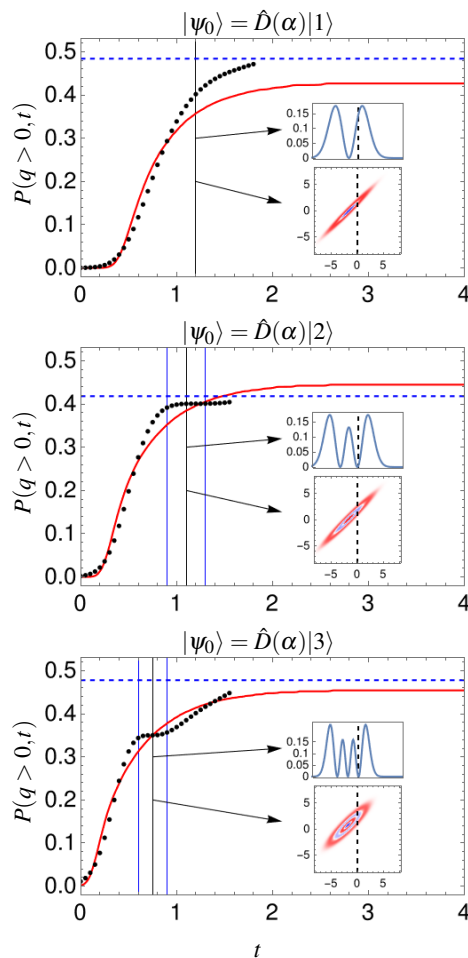


Figure 4. Probability $P(q > 0, t)$ of finding the particle at the right side of the inverted oscillator. The initial states are the displaced Fock state $D(\alpha)|n\rangle$ with displacement parameter $\alpha = \frac{1}{\sqrt{2}}(-3 + 2.5i)$. In the inverted oscillator (1) all states have the same mean energy $\bar{E} = -1.375$. The solid red curve shows the transmission probability from the Gaussian approximation + TWA method (13), while the black points show the exact marginal probability (8). The blue dashed line represents the probability $P_0(E > 0)$. The blue vertical lines indicate the start and end of the short-time plateaus. The insets show the Wigner function (6) and the marginal distribution (7) at the time indicated by the vertical black line.

of above-barrier components. In contrast, the TWA simulations cannot access the classically forbidden region Ω_r , since the semiclassical trajectories remain disconnected (see Figure 1). This penetration into the classically forbidden region is therefore a genuinely quantum phenomenon that cannot be reproduced within any classical phase-space description.

A natural question arising from the dynamics of the displaced Fock states shown in Figure 5 is whether the emergence of quantum interference modifies the behavior of the transmission probability over time. Figure 6 displays the time evolution of the transmission probability $P(q > 0, t)$ for several initial displaced Fock states $D(\alpha)|n\rangle$. In the presence of the Kerr nonlinearity, the displacement parameter is adjusted

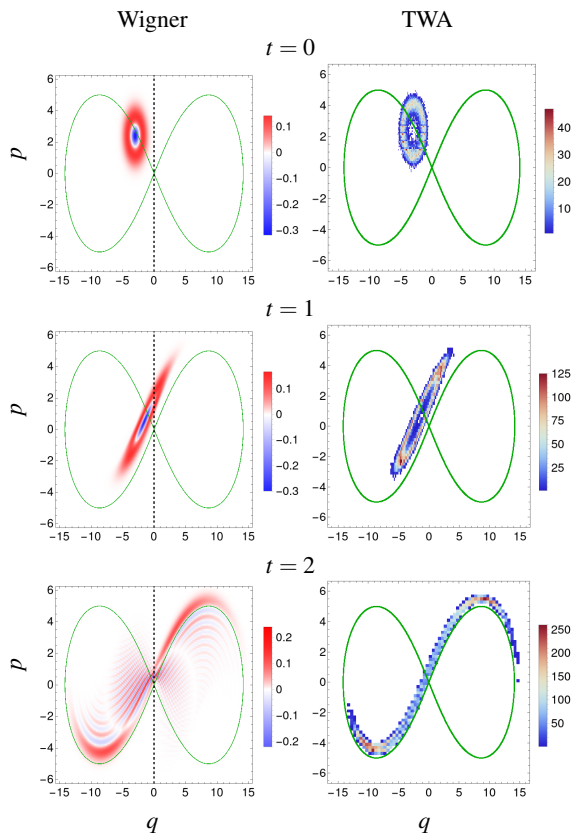


Figure 5. (Left column) Dynamics of the Wigner function of the initial displaced state $D(\alpha)|1\rangle$ with displacement parameter $\alpha = \frac{1}{\sqrt{2}}(-3 + 2.395i)$ in the Kerr inverted oscillator. On the left column the exact Wigner function and on the right column the TWA simulations with $N = 10^4$ points. The green line is the separatrix. For all figures the driving strength $\varepsilon_2 = 1/2$ and the Kerr non-linearity $K = 10^{-2}$ are fixed. The right side of the separatrix, Ω_r , is a classically forbidden region that is inaccessible to the TWA method.

so that all states share the same mean energy, $E \approx -0.79$. Because the Kerr nonlinearity is weak, the dynamics closely resemble those of the inverted oscillator, including the short-time plateaus that appear when regions of the Wigner function negativity cross the barrier. Owing to the bounded phase space, the integral defining the transmission probability (8) converges at longer times, allowing for meaningful asymptotic comparisons.

For coherent states ($n = 0$), the agreement between the exact and TWA transmission probabilities remains remarkably good. For displaced Fock states with $n \neq 0$, the asymptotic transmission probabilities show systematic but generally small deviations from the exact quantum results. In most cases, the TWA underestimates the transmission probability, although in certain instances it slightly overestimates it.

More importantly, it is confirmed that the exact transmission probability $P(x > 0, t)$ never exceeds the initial positive-energy fraction $P_0(E > 0)$. This result demonstrates that, although quantum interference develops in the classically forbidden regions, the combined contribution of positive and

negative interference patterns cancels out and the total transmission remains bounded by $P_0(E > 0)$. According to this result, the maximum possible value of the transmission probability is already encoded in the initial state.

With regards to the TWA simulations, it is the inability of the Gaussian approximation (17) to accurately replicate the nonclassical initial state that ultimately leads to discrepancies in the predicted transmission probability.

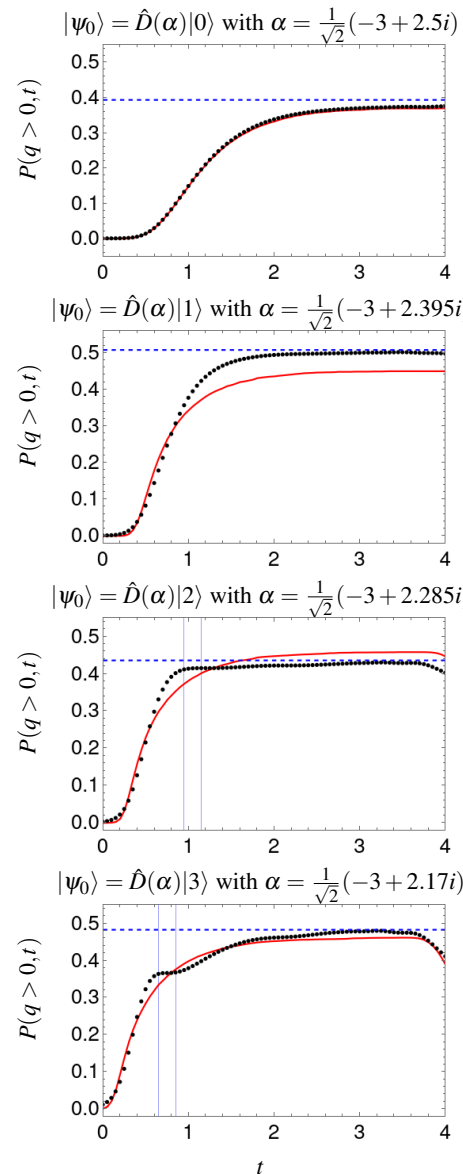


Figure 6. Probability $P(q > 0, t)$ of finding the particle on the right side of the Kerr inverted oscillator, starting from displaced Fock states $\hat{D}(\alpha)|n\rangle$. All initial states have $\bar{q} = -3$ and mean energy $E \approx -0.79$, below the barrier threshold. The solid red curve shows the transmission probability from the TWA method (13), black points denote the exact marginal probability (8), and the blue dashed line the probability $P_0(E > 0)$. The vertical blue line indicates the onset and end of the short-time plateaus. Parameters: $\varepsilon = 1/2$, $K = 10^{-2}$. The analysis is terminated at $t = 3$, before the states return to the left side of the oscillator.

Figure 8 panel (a) shows the energy variance $\sigma_H = \sqrt{\langle \hat{H}^2 \rangle - \langle \hat{H} \rangle^2}$ of the initial displaced Fock states presented in Figure 6. The variance increases monotonically with the Fock index n , indicating that higher-order Fock states possess broader energy distributions. In contrast, the corresponding positive-energy fraction $P_0(E > 0)$, shown in Figure 8 panel (b), exhibits a nonmonotonic dependence on n . This behavior arises because $P_0(E > 0)$ is governed by the relative position of the positive and negative lobes of the Wigner function with respect to the separatrix. Consequently, while a larger energy variance generally favors transmission, the detailed interference pattern of each displaced Fock state also plays a crucial role. The interplay between the energy spread and the fine structure of the Wigner function explains why the transmission probability does not simply scale with n but instead exhibits an oscillatory dependence, in which quantum interference fringes alternately enhance or degrade the transmission. Similar behavior — namely, the modulation of transmission by quantum interference structures — has been observed in single-molecule transistors, where destructive interference between two conduction channels suppresses leakage and thereby enhances device performance [82].

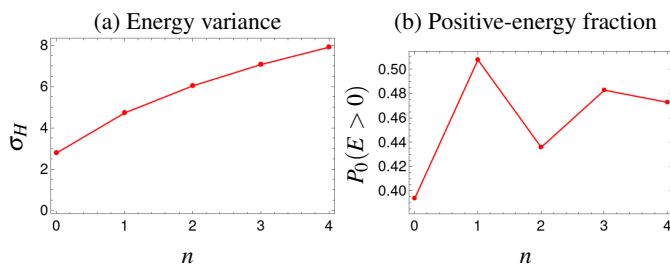


Figure 7. (a) Variance σ_H of the Hamiltonian (3) and (b) Positive-energy fraction $P_0(E > 0)$ for the initial states in Figure 6 as a function of the Fock index.

In Figure 8 panel (a) we show that the discrepancy between the TWA and the exact quantum results decreases and eventually vanishes as the mean energy approaches the barrier top. Moreover, Figure 8 panel (b) illustrates that the agreement between the TWA and the exact results systematically improves with increasing Fock index n of the initial state. This trend is consistent with the expected validity of the Gaussian approximation [78]. As the Fock index increases, the Wigner function approaches a narrow, nearly Gaussian ring in phase space, thereby reducing the influence of interference fringes and enhancing the accuracy of the semiclassical description.

The nonzero volume of the Wigner function in the classically forbidden region Ω_r , highlights the limitations of the classical simulation. Figure 9 shows the absolute volume of the Wigner function in Ω_r as a function of time for different initial Fock states. These results confirm that the ability of the states to penetrate into the classically forbidden region increases with the initial Fock index n . Furthermore, the number of sign changes observed in the slice of the Wigner function along $p = 0$ quantify the interference pattern within the classically forbidden region.

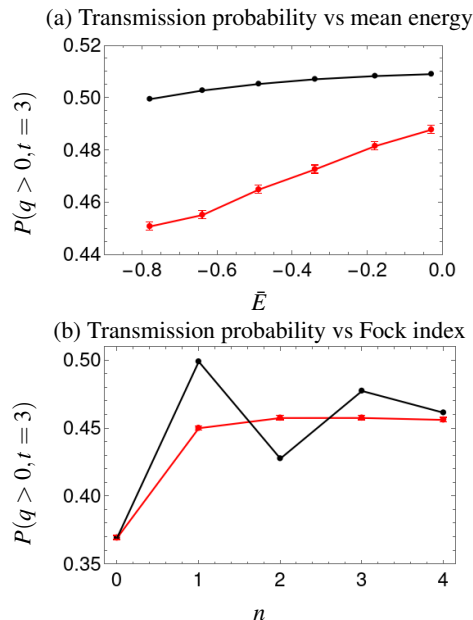


Figure 8. (a) Transmission probability $P(q > 0, t = 3)$ for the displaced Fock state $\hat{D}(\alpha)|1\rangle$ in the inverted oscillator with $\varepsilon_2 = 1/2$ and Kerr nonlinearity $K = 10^{-2}$, shown as a function of the mean energy. The displacement parameter is $\alpha = \frac{1}{\sqrt{2}}(-3 + ip)$, with the imaginary part varied so that the mean energy approaches the barrier top $E_c = 0$. The probability is evaluated at $t = 3$, before the state reflects back to the left side of the inverted oscillator. (b) Transmission probability $P(q > 0, t = 3)$ for displaced Fock states $\hat{D}(\alpha)|n\rangle$ in the same system, shown as a function of the Fock index n . All initial states are prepared with mean energy $\bar{E} = -0.79$ and mean position $\bar{q} = -3$. In both panels, The red points represents the transmission probability from the TWA method (13), while the black points show the exact marginal probability (8).

IV. CONCLUSIONS

We have investigated the transmission of Fock states through an inverted oscillator, both with and without Kerr nonlinearity. For the analysis we concentrate on states with average energies below the top of the inverted oscillator. It was used a Gaussian approximation to replicate the Fock states in the classical phase space and the TWA to track the dynamics. The semiclassical results were compared against those from the Wigner function and the marginals probabilities. For coherent states, which have strictly positive Wigner functions, the transmission probability shows good agreement between the TWA and the exact marginal probabilities. In contrast, for displaced Fock states exhibiting substantial Wigner negativity, clear discrepancies arise even at short times. In particular, short-time plateaus emerge when negative regions of the Wigner function (or, equivalently, zeros of the probability distribution) cross the inverted oscillator barrier. These plateaus cannot be reproduced semiclassically and thus constitute a genuine quantum effect. At longer times in the inverted oscillator, the rapid delocalization of the states prevents convergence of the transmission probability, leaving

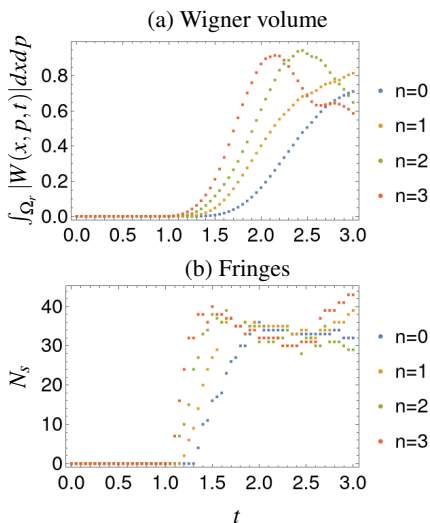


Figure 9. (a) Volume of the absolute Wigner function in the classically forbidden region Ω_r as a function of time. (b) Number N_s of sign changes in the slice of the Wigner function $W(x, 0, t)$ along momentum and within the classically forbidden region Ω_r . The number of sign changes quantify the fringe structure. The color of the points indicate the Fock index of the initial displaced Fock $|\psi_0\rangle = \hat{D}(\alpha)|n\rangle$ states. The displacement parameters are chosen to keep the mean energy fixed at $\bar{E} \approx -0.79$ (see Figure 6). For all figures the driving strength $\varepsilon_2 = 1/2$ and the Kerr non-linearity $K = 10^{-2}$ are fixed.

the asymptotic comparisons inconclusive.

Introducing a Kerr nonlinearity effectively confines the phase space and enables the analysis to be extended to longer times. However, the Kerr nonlinearities also introduce forces that modify the negativity of the states. At short times the states are squeezed just as they are in the pure inverted oscillator. At longer times, the dynamics follow the curvature of the separatrix while interference fringes develop within the classically forbidden region. This is the second phenomenon impossible to simulate in the classical phase space by the TWA approximation since the trajectories are disconnected. The transmission probabilities from the TWA and the exact marginals exhibit systematic discrepancies that decrease as the index of the Fock state increase or as the average energy approaches the critical energy (the barrier top).

Finally, we find that the exact transmission probability

$P(x > 0, t)$ never exceeds the initial positive-energy fraction $P_0(E > 0)$. This demonstrates that the maximum attainable transmission is already encoded in the energetic structure of the initial Fock state. Because Fock states cannot be faithfully replicated within a classical phase-space framework, the semiclassical approximations remain effectively unaware of this bound.

V. NUMERICAL DETAIL AND DATA AVAILABILITY

All codes, scripts and data needed to reproduce the results in this manuscript are available online [83]

<https://github.com/djuliannader/InvertedOscillator>

The exact Wigner functions (6) were computed using the *QuantumOptics.jl* framework [84], and the integrals for the transmission probabilities (8) were evaluated with the Julia package *HCubature* [85]. The Fock basis was truncated at $n_{\max} = 100$, and the relative error tolerance for the integrals was set to 10^{-6} . The integration domain was chosen as $q \in [-15, 15]$ and $p \in [-15, 15]$. As for the Gaussian approximation + TWA we used $N = 10^5$ sampling points to replicate the initial states. The canonical equations (11) were solved numerically using *NDSolve* from *Mathematica* [86]. The statistical error for the transmission probability (13) is estimated as usual for binomial distributions [87]

$$\sigma = \sqrt{\frac{P(q > 0, t)(1 - P(q > 0, t))}{N}}. \quad (18)$$

Error bars are only visible at the scale of Figure 8. When a Kerr nonlinearity is introduced $K > 0$, the Gaussian approximation systematically overestimates the mean energy. To compensate for this shift, we manually adjust the initial average momentum so that the states in the Gaussian approximation have the same mean energy as in the exact solution.

VI. ACKNOWLEDGMENTS

D.J.N. acknowledges financial support from the Programme Johannes Amos Comenius under the Ministry of Education, Youth and Sports of the Czech Republic reg. no. CZ.02.01.01/00/22_008/0004649 D.J.N. thanks D. W. Moore and S. Lerma-Hernández for useful discussions.

-
- [1] E. Merzbacher, The early history of quantum tunneling, *Physics Today* **55**, 44 (2002).
 - [2] F. Hund, Zur deutung der molekelspektren. i, *Zeitschrift für Physik* **40**, 742 (1927).
 - [3] L. Nordheim, Zur theorie der thermischen emission und der reflexion von elektronen an metallen, *Zeitschrift für Physik* **46**, 833 (1928).
 - [4] G. Gamow, The quantum theory of nuclear disintegration, *Nature* **122**, 805 (1928).
 - [5] G.-R. Feng, Y. Lu, L. Hao, F.-H. Zhang, and G.-L. Long, Experimental simulation of quantum tunneling in small systems, *Scientific Reports* **3**, 2232 (2013).
 - [6] M. H. Devoret, J. M. Martinis, and J. Clarke, Measurements of macroscopic quantum tunneling out of the zero-voltage state of a current-biased josephson junction, *Physical review letters* **55**, 1908 (1985).
 - [7] M. Fiske and I. Giaever, Superconductive tunneling, *Proceedings of the IEEE* **52**, 1155 (1964).

- [8] R. Ramos, D. Spierings, I. Racicot, and A. M. Steinberg, Measurement of the time spent by a tunnelling atom within the barrier region, *Nature* **583**, 529 (2020).
- [9] M. Zendra, F. Borgonovi, G. L. Celardo, and S. Gurvitz, Many-body tunneling in a double-well potential, *Physical Review A* **110**, 062222 (2024).
- [10] R. Ferreira and G. Bastard, Tunnelling and relaxation in semiconductor double quantum wells, *Reports on Progress in Physics* **60**, 345 (1997).
- [11] D.-Y. Song, Localization or tunneling in asymmetric double-well potentials, *Annals of Physics* **362**, 609 (2015).
- [12] D. Braun and J. Martin, Spontaneous emission from a two-level atom tunneling in a double-well potential, *Physical Review A—Atomic, Molecular, and Optical Physics* **77**, 032102 (2008).
- [13] H. Hasegawa, Gaussian wavepacket dynamics and quantum tunneling in asymmetric double-well systems, *Physica A: Statistical Mechanics and its Applications* **392**, 6232 (2013).
- [14] M. A. P. Reynoso, D. J. Nader, J. Chávez-Carlos, B. E. Ordaz-Mendoza, R. G. Cortiñas, V. S. Batista, S. Lerma-Hernández, F. Pérez-Bernal, and L. F. Santos, Quantum tunneling and level crossings in the squeeze-driven kerr oscillator, *Phys. Rev. A* **108**, 033709 (2023).
- [15] M. Marthaler and M. Dykman, Quantum interference in the classically forbidden region: A parametric oscillator, *Physical Review A—Atomic, Molecular, and Optical Physics* **76**, 010102 (2007).
- [16] D. J. Nader, C. A. González-Rodríguez, and S. Lerma-Hernández, Avoided crossings and dynamical tunneling close to excited-state quantum phase transitions, *Phys. Rev. E* **104**, 064116 (2021).
- [17] G. Chen and J. Liang, Unconventional quantum phase transition in the finite-size lipkin–meshkov–glick model, *New Journal of Physics* **8**, 297 (2006).
- [18] G. Milburn, J. Corney, E. M. Wright, and D. Walls, Quantum dynamics of an atomic bose-einstein condensate in a double-well potential, *Physical Review A* **55**, 4318 (1997).
- [19] S. Zöllner, H.-D. Meyer, and P. Schmelcher, Tunneling dynamics of a few bosons in a double well, *Physical Review A—Atomic, Molecular, and Optical Physics* **78**, 013621 (2008).
- [20] N. Kluksdahl, A. Kriman, and D. Ferry, Wigner function simulation of quantum tunneling, *Superlattices and Microstructures* **4**, 127 (1988).
- [21] K. G. Kay, Time-dependent semiclassical tunneling through barriers, *Phys. Rev. A* **88**, 012122 (2013).
- [22] K. L. Jensen, J. L. Lebowitz, J. M. Riga, D. A. Shiffler, and R. Seviour, Wigner wave packets: Transmission, reflection, and tunneling, *Phys. Rev. B* **103**, 155427 (2021).
- [23] C. S. Tautermann, A. F. Voegelé, T. Loerting, and K. R. Liedl, An accurate semiclassical method to predict ground-state tunneling splittings, *The Journal of chemical physics* **117**, 1967 (2002).
- [24] G. Rastelli, Semiclassical formula for quantum tunneling in asymmetric double-well potentials, *Physical Review A—Atomic, Molecular, and Optical Physics* **86**, 012106 (2012).
- [25] L. Aragón-Muñoz, G. Chacón-Acosta, and H. Hernandez-Hernandez, Effective quantum tunneling from a semiclassical momentous approach, *International Journal of Modern Physics B* **34**, 2050271 (2020).
- [26] J. Le Deunff, A. Mouchet, and P. Schlagheck, Semiclassical description of resonance-assisted tunneling in one-dimensional integrable models, *Phys. Rev. E* **88**, 042927 (2013).
- [27] M. Hillery, R. F. O’Connell, M. O. Scully, and E. P. Wigner, Distribution functions in physics: Fundamentals, *Physics reports* **106**, 121 (1984).
- [28] Y. Lu, I. Strandberg, F. Quijandría, G. Johansson, S. Gasparinetti, and P. Delsing, Propagating wigner-negative states generated from the steady-state emission of a superconducting qubit, *Physical Review Letters* **126**, 253602 (2021).
- [29] S. Rahimi-Keshari, T. C. Ralph, and C. M. Caves, Sufficient conditions for efficient classical simulation of quantum optics, *Physical Review X* **6**, 021039 (2016).
- [30] Y. Xiang, S. Liu, J. Guo, Q. Gong, N. Treps, Q. He, and M. Walschaers, Distribution and quantification of remotely generated wigner negativity, *npj Quantum Information* **8**, 21 (2022).
- [31] F. Toscano, D. A. R. Dalvit, L. Davidovich, and W. H. Zurek, Sub-planck phase-space structures and heisenberg-limited measurements, *Phys. Rev. A* **73**, 023803 (2006).
- [32] Y. L. Lin and O. C. O. Dahlsten, Necessity of negative wigner function for tunneling, *Phys. Rev. A* **102**, 062210 (2020).
- [33] C. Chen and S. Zhou, Insights into quantum tunneling via a phase-space approach, *Phys. Rev. A* **109**, 032227 (2024).
- [34] I. F. Valtierra and A. B. Klimov, Tunneling currents in the hyperbolic phase space, *Entropy* **26**, 639 (2024).
- [35] A. Ono, Phase-space consideration on barrier transmission in a time-dependent variational approach with superposed wave packets, *Physics Letters B* **826**, 136931 (2022).
- [36] G. Breitenbach, S. Schiller, and J. Mlynek, Measurement of the quantum states of squeezed light, *Nature* **387**, 471 (1997).
- [37] U. Leonhardt and H. Paul, Measuring the quantum state of light, *Progress in Quantum Electronics* **19**, 89 (1995).
- [38] A. I. Lvovsky, H. Hansen, T. Aichele, O. Benson, J. Mlynek, and S. Schiller, Quantum state reconstruction of the single-photon fock state, *Physical Review Letters* **87**, 10.1103/PhysRevLett.87.050402 (2001).
- [39] J. Park, Y. Lu, J. Lee, Y. Shen, K. Zhang, S. Zhang, M. S. Zubairy, K. Kim, and H. Nha, Revealing nonclassicality beyond Gaussian states via a single marginal distribution, *Proceedings of the National Academy of Science* **114**, 891 (2017), [arXiv:1702.01387 \[quant-ph\]](https://arxiv.org/abs/1702.01387).
- [40] A. Polkovnikov, Phase space representation of quantum dynamics, *Annals of Physics* **325**, 1790 (2010).
- [41] J. Schachenmayer, A. Pikovski, and A. M. Rey, Many-body quantum spin dynamics with monte carlo trajectories on a discrete phase space, *Phys. Rev. X* **5**, 011022 (2015).
- [42] P. D. Drummond and C. W. Gardiner, Generalised p-representations in quantum optics, *Journal of Physics A: Mathematical and General* **13**, 2353 (1980).
- [43] J. F. Corney and M. K. Olsen, Non-gaussian pure states and positive wigner functions, *Phys. Rev. A* **91**, 023824 (2015).
- [44] A. Kenfack and K. Życzkowski, Negativity of the wigner function as an indicator of non-classicality, *Journal of Optics B: Quantum and Semiclassical Optics* **6**, 396 (2004).
- [45] X.-B. Wang, T. Hiroshima, A. Tomita, and M. Hayashi, Quantum information with gaussian states, *Physics reports* **448**, 1 (2007).
- [46] B. Wielinga and G. J. Milburn, Quantum tunneling in a kerr medium with parametric pumping, *Phys. Rev. A* **48**, 2494 (1993).
- [47] S. Marti, U. von Lüpke, O. Joshi, Y. Yang, M. Bild, A. Omani, Y. Chu, and M. Fadel, Quantum squeezing in a nonlinear mechanical oscillator, *Nature Physics* , 1 (2024).
- [48] X. He, Y. Lu, D. Bao, H. Xue, W. Jiang, Z. Wang, A. Roudsari, P. Delsing, J. Tsai, and Z. Lin, Fast generation of schrödinger cat states using a kerr-tunable superconducting resonator, *Nature*

- ture communications **14**, 6358 (2023).
- [49] G. Barton, Quantum mechanics of the inverted oscillator potential, *Annals of Physics* **166**, 322 (1986).
- [50] C. Yuce, Quantum inverted harmonic potential, *Physica Scripta* **96**, 105006 (2021).
- [51] F. Ullinger, M. Zimmermann, and W. P. Schleich, The logarithmic phase singularity in the inverted harmonic oscillator, *AVS Quantum Science* **4** (2022).
- [52] A. Albrecht, P. Ferreira, M. Joyce, and T. Prokopec, Inflation and squeezed quantum states, *Physical Review D* **50**, 4807 (1994).
- [53] S. Wang, S. Chen, and J. Jing, Classical-quantum correspondence for inverted harmonic oscillator (2023), [arXiv:2211.10078 \[quant-ph\]](https://arxiv.org/abs/2211.10078).
- [54] P. Romatschke, Out-of-time-ordered-correlators for the pure inverted quartic oscillator: classical chaos meets quantum stability, *Journal of High Energy Physics* **2024**, 1 (2024).
- [55] M. Maamache and J. R. Choi, Quantum-classical correspondence for the inverted oscillator, *Chinese Physics C* **41**, 113106 (2017).
- [56] D. F. Walls and J. D. Harvey, *Quantum Optics VI: Proceedings of the Sixth International Symposium on Quantum Optics, Rotorua, New Zealand, January 24–28, 1994*, Vol. 77 (Springer Science & Business Media, 2012).
- [57] S. Puri, S. Boutin, and A. Blais, Engineering the quantum states of light in a kerr-nonlinear resonator by two-photon driving, *npj Quantum Information* **3**, 18 (2017).
- [58] J. Chávez-Carlos, T. L. Lezama, R. G. Cortiñas, J. Venkatraman, M. H. Devoret, V. S. Batista, F. Pérez-Bernal, and L. F. Santos, Spectral kissing and its dynamical consequences in the squeeze-driven kerr oscillator, *npj Quantum Information* **9**, 76 (2023).
- [59] Y. Cai, X. Deng, L. Zhang, Z. Ni, J. Mai, P. Huang, P. Zheng, L. Hu, S. Liu, Y. Xu, *et al.*, Quantum squeezing amplification with a weak kerr nonlinear oscillator, [arXiv preprint arXiv:2503.08197](https://arxiv.org/abs/2503.08197) (2025).
- [60] J. Venkatraman, R. G. Cortiñas, N. E. Frattini, X. Xiao, and M. H. Devoret, A driven kerr oscillator with two-fold degeneracies for qubit protection, *Proceedings of the National Academy of Sciences* **121**, e2311241121 (2024).
- [61] S. Rebic, S. Tan, A. Parkins, and D. Walls, Large kerr nonlinearity with a single atom, *Journal of Optics B: Quantum and Semiclassical Optics* **1**, 490 (1999).
- [62] M. A. P. Reynoso, E. M. Signor, J. Khalouf-Rivera, A. D. Ribeiro, F. Pérez-Bernal, and L. F. Santos, Phase transitions, symmetries, and tunneling in kerr parametric oscillators, [arXiv preprint arXiv:2504.15347](https://arxiv.org/abs/2504.15347) (2025).
- [63] A. Grimm, N. E. Frattini, S. Puri, S. O. Mundhada, S. Touzard, M. Mirrahimi, S. M. Girvin, S. Shankar, and M. H. Devoret, Stabilization and operation of a kerr-cat qubit, *Nature* **584**, 205 (2020).
- [64] S. Boutin, D. M. Toyli, A. V. Venkatramani, A. W. Eddins, I. Siddiqi, and A. Blais, Effect of higher-order nonlinearities on amplification and squeezing in josephson parametric amplifiers, *Phys. Rev. Appl.* **8**, 054030 (2017).
- [65] F. Iachello, R. G. Cortiñas, F. Pérez-Bernal, and L. F. Santos, Symmetries of the squeeze-driven kerr oscillator, *Journal of Physics A: Mathematical and Theoretical* **56**, 495305 (2023).
- [66] K. Holmes, W. Rehman, S. Malzard, and E.-M. Graefe, Husimi dynamics generated by non-hermitian hamiltonians, *Physical Review Letters* **130**, 157202 (2023).
- [67] M. Marthaler and M. Dykman, Switching via quantum activation: A parametrically modulated oscillator, *Physical Review A—Atomic, Molecular, and Optical Physics* **73**, 042108 (2006).
- [68] A. C. Oliveira, J. G. Peixoto de Faria, and M. C. Nemes, Quantum-classical transition of the open quartic oscillator: The role of the environment, *Phys. Rev. E* **73**, 046207 (2006).
- [69] D. Nader and E. Serrano-Ensástiga, Critical energies and wigner functions of the stationary states of the bose einstein condensates in a double-well trap, *Advanced Quantum Technologies* , 2400451 (2025).
- [70] D. Nader, J. Hernández-González, H. Vázquez-Sánchez, and S. Lerma-Hernández, Manifestation of classical instability in the quantum density of states of a double well potential, *Physics Letters A* **481**, 129014 (2023).
- [71] S. Deléglise, I. Dotsenko, C. Sayrin, J. Bernu, M. Brune, J.-M. Raimond, and S. Haroche, Reconstruction of non-classical cavity field states with snapshots of their decoherence, *Nature* **455**, 510—514 (2008).
- [72] M. Hofheinz, E. Weig, M. Ansmann, R. C. Bialczak, E. Lucero, M. Neeley, A. O’Connell, H. Wang, J. M. Martinis, and A. Cleland, Generation of fock states in a superconducting quantum circuit, *Nature* **454**, 310—314 (2008).
- [73] W. B. Case, Wigner functions and Weyl transforms for pedestrians, *American Journal of Physics* **76**, 937 (2008).
- [74] E. Colomé, Z. Zhan, and X. Oriols, Comparing wigner, husimi and bohmian distributions: which one is a true probability distribution in phase space?, *Journal of Computational Electronics* **14**, 894 (2015).
- [75] J. Teske, M. Besbes, B. Okhrimenko, and R. Walser, Mean-field wigner function of bose–einstein condensates in the thomas–fermi limit, *Physica Scripta* **93**, 124004 (2018).
- [76] G. Adesso, S. Ragy, and A. R. Lee, Continuous variable quantum information: Gaussian states and beyond, *Open Systems & Information Dynamics* **21**, 1440001 (2014).
- [77] C. Gardiner and P. Zoller, *Quantum noise: a handbook of Markovian and non-Markovian quantum stochastic methods with applications to quantum optics* (Springer Science & Business Media, 2004).
- [78] M. Olsen and A. Bradley, Numerical representation of quantum states in the positive-p and wigner representations, *Optics Communications* **282**, 3924 (2009).
- [79] S. Koh, Wigner Function of a Time-dependent Inverted Harmonic Oscillator, *New Phys. Sae Mulli* **73**, 74 (2023).
- [80] V. Bagrov, D. Gitman, E. Macedo, and A. Pereira, Coherent states of inverse oscillators and related problems, *Journal of Physics A: Mathematical and Theoretical* **46**, 325305 (2013).
- [81] J. Glaisher, Xxxii. on a class of definite integrals, *The London, Edinburgh, and Dublin Philosophical Magazine and Journal of Science* **42**, 294 (1871), <https://doi.org/10.1080/14786447108640568>.
- [82] Z. Chen, I. M. Grace, S. L. Woltering, L. Chen, A. Gee, J. Baugh, G. A. D. Briggs, L. Bogani, J. A. Mol, C. J. Lambert, *et al.*, Quantum interference enhances the performance of single-molecule transistors, *Nature Nanotechnology* **19**, 986 (2024).
- [83] D. Nader, Inverted oscillator, <https://github.com/djuliannader/InvertedOscillator> (2025).
- [84] S. Krämer, D. Plankensteiner, L. Ostermann, and H. Ritsch, *Quantumoptics.jl*: A julia framework for simulating open quantum systems, *Computer Physics Communications* **227**, 109 (2018).
- [85] S. G. Johnson, The HCubature.jl package for multi-dimensional adaptive integration in Julia, <https://github.com/JuliaMath/HCubature.jl> (2017).
- [86] Wolfram Research, *NDSolve*, Wolfram Research, Inc., Champaign, Illinois (2025), version 14.0, <https://reference>.

wolfram.com/language/ref/NDSolve.html.

- [87] G. Casella and R. Berger, *Statistical inference* (Chapman and Hall/CRC, 2024).